Analysis of the Dynamical Behaviour of Spinning Annular Disks with Various Boundary Conditions

Hilal Koç[a], Ömer Ekim Genel[a], Mertol Tüfekci[b] and Ekrem Tüfekci[a]*

[a]*Faculty of Mechanical Engineering, Istanbul Technical University, Istanbul, TURKEY;*
[b]*Department of Mechanical Engineering, Imperial College London, London SW7 2AZ, UNITED KINGDOM*

*Corresponding Author: tufekcie@itu.edu.tr

Analysis of the Dynamical Behaviour of Spinning Annular Disks with Various Boundary Conditions

ABSTRACT

This study investigates the vibration characteristics of spinning annular disks with various boundary conditions aiming to investigate the effect of radius ratio parameter and the rotation speed on natural frequencies of a spinning disk analytically for nine different types of boundary conditions. The stress distributions on the disks are obtained for all boundary conditions. The Galerkin method is employed with polynomial functions as approximate displacement functions. Analytical results are presented and compared to the results of the finite element analyses as well as experimental ones.

Keywords: Spinning disk; transverse vibration; analytical solution; Galerkin method; free vibration

Subject classification codes: Structural Dynamics/Vibration; Gyrodynamics; Plates and Grillages

1. INTRODUCTION

Since being utilised by the vast majority of machinery, rotating plates are one of the ongoing research fields in engineering. Aero-engines, turbines and fans in power plants, flywheels, grinding wheels, cutting tool types of equipment, gears in machinery automotive and train wheels in transportation and as a more modern instance, hard disks in informatics are among the most common examples (Kirkhope and Wilson 1976, Sun *et al.* 2020, Tufekci *et al.* 2020, Tuzzi *et al.* 2020). The engineers must understand the dynamics of these structures to prevent any failure. Especially, since these structures perform critical duties at high speeds, hard disk drives draw the attention of engineers. The contact forces between the disk and read-write head can overload the system due to excessive vibrations hindering the performance of the system (Huang and Lin 2008, Tufekci *et al.* 2019). Therefore, the dynamical characteristics of rotating plates should

be accurately considered.

There are plenty of works about vibrations of spinning annular plates. Lamb and Southwell (Lamb and Southwell 1921) present the first analytical study that the spinning disk is modelled by using linear elastic theory without any bending stiffness.

The majority of the analytical research, that concentrates on obtaining natural frequencies and mode shapes, uses Rayleigh-Ritz (Southwell 1922, Mote 1965, Ramaiah 1981, Koo 2006, Kang 2017) and Galerkin methods (Luo and Mote 2000, Pei and Tan 2009), perturbation techniques (Mignolet *et al.* 1996), the method of multiple scales (Nayfeh *et al.* 2001), the Frobenius method (Maretic *et al.* 2015). Most of the recent studies on the topic are focused on functionally graded materials (FGMs) (Güven and Çelik 2001, Yıldırım 2018).

There are also studies about non-classical boundary conditions in the literature. Lyu et al. (Lyu *et al.* 2019) present an analytical study on free in-plane vibrations of spinning circular panels under elastic boundary constraints. Yano and Kotera (Yano and Kotera 1991) study the unstable vibrations of rotating disks with elastic supports. Parker and Sathe (Parker and Sathe 1999a, 1999b) handle the effect of the presence of an elastic spindle on the mechanics of rotating disks. Amabili et al. (Amabili *et al.* 1997) investigate the effect of non-uniform boundary conditions focusing on the applications of bolted plates. Another remarkable study conducted by Shafei et al. (Shafei *et al.* 2021) explores the nonlinear transient vibrations of viscoelastic plates.

Besides these analytical studies, there are numerous works that are interested in fields other than stability considerations (Kutug *et al.* 2003, Oldac *et al.* 2017, Tufekci *et al.* 2018), numerical (Barasch and Chen 1972, Kim and Lee 1988, Nguyen-Thanh *et al.* 2009) and experimental approaches in the literature (Xu and Guo 2003, Kajiwara and Hosoya 2013, Bashmal *et al.* 2016, Tufekci *et al.* 2017).

There are also new generation and novel methods developed to investigate the mechanics of various systems. Deep collocation is among those recently emerged methods which is used by Gue et al. (Guo *et al.* 2019) to model Kirchoff plates. Machine learning can also be used for similar purposes. Samaniego et al. (Samaniego *et al.* 2020) employ machine learning to solve partial differential equations taking advantage of an energy-based methodology. Alongside machine learning, probabilistic and statistical modelling methods recently become popular. Vu-Bac et al. (Vu-Bac *et al.* 2016) develop a workflow using statistical approach to explore the sensitivity of large systems that are computationally costly. Such methods can be used to analyse uncertainties in mechanical systems (Cicirello and Langley 2013, 2014, Panunzio *et al.* 2017).

Yıldırım (Yıldırım 2020) describe the best material distribution for pressurised annular disks. Some studies investigate free vibration analysis of annular plates by using the finite element method (FEM) (Mattikalli and Kurahatti 2018, Qin *et al.* 2018, Jaiman and Singh 2019).

The Galerkin method usually yields good results by using approximate functions with a limited number of unknowns. In the literature, the clamped-free boundary condition is often preferred in studies such as the one by Luo and Mote (Luo and Mote 2000). However, none of the present studies investigates all the classical boundary conditions using the same generalised Galerkin formulation. It is aimed to fill the gap in the literature with this study.

In this study, transverse free vibration problems of spinning disks are solved analytically under various boundary conditions. To obtain analytical results, the Galerkin method is utilised and as approximate displacement functions, polynomials are used by Tufekci et al. (Tufekci *et al.* 2018). The effect of the variation of radius ratio

(R_i/R_o) and the rotation speed on the dimensionless natural frequencies are investigated and obtained results are presented in 3D surface plots. Besides, the influence of the boundary conditions on the dynamics of the rotating disks is discussed. Also, the results are compared with those obtained by a finite element analysis. To the best of the authors' knowledge, no study investigating the disk vibrations with all classical boundary conditions using analytical approaches has hitherto been published. Even though, the analytical solutions are individually valid under certain assumptions and therefore they are not always generalisable as the numerical methods. This does not make analytical solutions less applicable. Besides, usage of analytical solutions is computationally cheaper and much more reliable without the necessity of validation compared to numerical methods which usually require strict validation studies. The main contribution of this study, therefore, is to develop an analytical formulation for rotating disks with several boundary conditions and to investigate the effects of various parameters on the dynamics of rotating disks.

2. FORMULATION AND ANALYSIS

2.1 General formulation of the problem

The equation of motion of a spinning annular disk can be ascribed in a frame of reference, which is stationary in space, by the utilization of the polar coordinates (r, φ) attached to the disk. R_o and R_i are the outer and inner radii, respectively, h is the thickness, Ω is the rotational speed. The well-known governing equation of motion can be pointed out as in Equation (1) which is only valid when the disk is thin, undergoing very small deflections and made of linearly elastic and isotropic material;

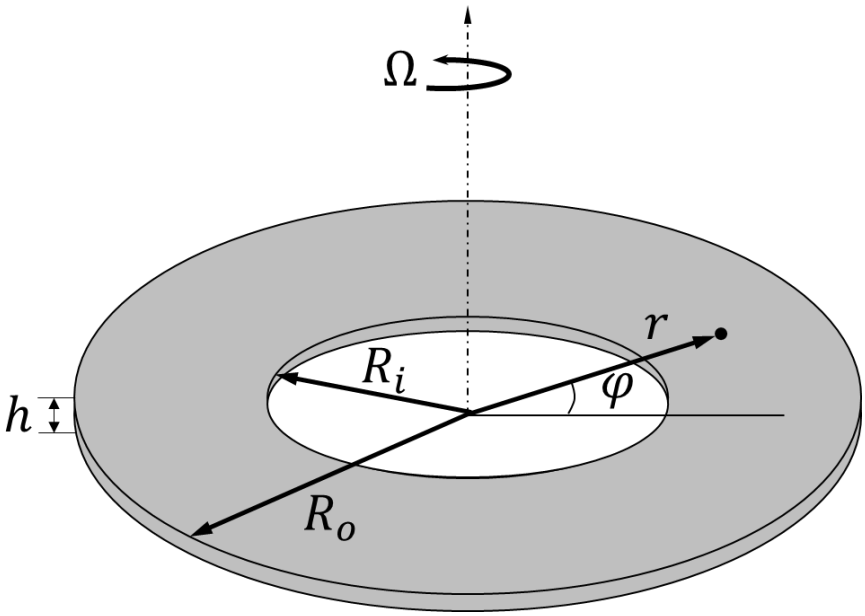


Figure 1. Schematic view of the spinning disk.

$$D\left(\frac{\partial^2}{\partial r^2}+\frac{1}{r}\frac{\partial}{\partial r}+\frac{1}{r^2}\frac{\partial^2}{\partial \varphi^2}\right)^2 w+\rho h\frac{\partial^2 w}{\partial t^2}-\frac{h}{r}\left[\frac{\partial}{\partial r}\left(\sigma_r r\frac{\partial w}{\partial r}\right)+\frac{1}{r}\sigma_\varphi\frac{\partial^2 w}{\partial \varphi^2}\right]=0 \quad (1)$$

where D is the flexural rigidity, $w(r,\varphi,t)$ is the lateral deflection of the disk, h is the thickness, ρ is the mass density of the material, t is the time, σ_r and σ_φ are the radial and tangential stresses.

In order to obtain the nondimensionalised form of Equation (1), the following relations are defined:

$$\tau=T\,t \quad R=\frac{r}{R_o} \quad W=\frac{w}{R_o} \quad \omega^*=\frac{\omega}{T} \quad \Omega^*=\frac{\Omega}{T} \quad (2)$$

Here, $\tau, R, W,\ \omega^*$ and Ω^* are dimensionless coefficients, ω is the natural frequency and T is defined as given in Equation (3);

$$T=\sqrt{\frac{D}{\rho h {R_o}^4}} \quad (3)$$

By substituting these dimensionless parameters into Equation (1), Equation (4)

is obtained:

$$\nabla^4 W + \frac{\partial^2 W}{\partial \tau^2} - \frac{(\Omega^*)^2}{{R_o}^2}\left[C_{rr}\frac{\partial^2 W}{\partial R^2} + C_{r\varphi}\frac{\partial W}{\partial R} + C_{\varphi\varphi}\frac{\partial^2 W}{\partial \varphi^2}\right] = 0 \quad (4)$$

Here, C_{rr}, $C_{r\varphi}$, and $C_{\varphi\varphi}$ are unknown coefficients related to the boundary conditions. These coefficients in the radial and tangential stress expressions are obtained using the Airy stress function for the axis-symmetric stress state depending on the boundary conditions. These can be formulated as shown in section 2.3.

The dimensionless transverse displacement function is defined in Equation (5);

$$W = \sum_{n=0}^{N}\sum_{m=0}^{M} a_{mn} R_{mn}(R)\sin[n\varphi + (n\Omega^* - \omega^*)\tau] \quad (5)$$

where, a_{mn} are the constants, $R_{mn}(R)$ are the shape functions, m and n are the nodal circle and nodal diameter in the mode shape. The presumed five-term polynomial is written in the form given in Equation (6);

$$R_{mn}(R) = X_{mn}^1 R^m + X_{mn}^2 R^{m+1} + X_{mn}^3 R^{m+2} + X_{mn}^4 R^{m+3} + X_{mn}^5 R^{m+4} \quad (6)$$

Making use of boundary conditions and the normalization condition, parameters of the approximate function are found. If $R_{mn}(R)$ is replaced into Equation (5) and Equation (4), Equation (7) is obtained;

$$\sum_{n=0}^{N}\sum_{m=0}^{M}\left\{\left(\frac{\partial^4 R_{mn}(R)}{\partial R^4} + \frac{2}{R}\frac{\partial^3 R_{mn}(R)}{\partial R^3} - \frac{1+2n^2}{R^2}\frac{\partial^2 R_{mn}(R)}{\partial R^2} + \frac{1+2n^2}{R^3}\frac{\partial R_{mn}(R)}{\partial R} + \frac{n^4-4n^2}{R^4}R_{mn}(R)\right) - R_{mn}(R)(n\Omega^* - \omega^*)^2 - \frac{(\Omega^*)^2}{{R_o}^2}\left[C_{rr}\frac{\partial^2 R_{mn}(R)}{\partial R^2} + C_{r\varphi}\frac{\partial R_{mn}(R)}{\partial R} - C_{\varphi\varphi}R_{mn}(R)\,n^2\right]\right\} a_{mn}\sin[n\varphi + (n\Omega^* - \omega^*)\tau] = 0 \quad (7)$$

The term in the parenthesis has to be equal to zero since $\sin[n\varphi + (n\Omega^* - \omega^*)\tau]$

cannot be equal to zero. Therefore, the following equation is obtained;

$$\sum_{n=0}^{N}\sum_{m=0}^{M}\left\{\left(\frac{\partial^4 R_{mn}(R)}{\partial R^4}+\frac{2}{R}\frac{\partial^3 R_{mn}(R)}{\partial R^3}-\frac{1+2n^2}{R^2}\frac{\partial^2 R_{mn}(R)}{\partial R^2}+\frac{1+2n^2}{R^3}\frac{\partial R_{mn}(R)}{\partial R}+\right.\right.$$

$$\left.\frac{n^4-4n^2}{R^4}R_{mn}(R)\right)-R_{mn}(R)(n\Omega^*-\omega^*)^2-\frac{(\Omega^*)^2}{{R_o}^2}\left[C_{rr}\frac{\partial^2 R_{mn}(R)}{\partial R^2}+C_{r\varphi}\frac{\partial R_{mn}(R)}{\partial R}-\right.$$

$$\left.\left.C_{\varphi\varphi}R_{mn}(R)\,n^2\right]\right\}a_{mn}=0 \qquad (8)$$

For the solution of this equation, the Galerkin method is used. The weighted residual is expressed as in Equation (9);

$$\int_0^{2\pi}\int_{\frac{R_i}{R_o}}^{1}\sum_{n=0}^{N}\sum_{m=0}^{M}\left\{\left(\frac{\partial^4 R_{mn}(R)}{\partial R^4}+\frac{2}{R}\frac{\partial^3 R_{mn}(R)}{\partial R^3}-\frac{1+2n^2}{R^2}\frac{\partial^2 R_{mn}(R)}{\partial R^2}+\frac{1+2n^2}{R^3}\frac{\partial R_{mn}(R)}{\partial R}+\right.\right.$$

$$\left.\frac{n^4-4n^2}{R^4}R_{mn}(R)\right)-R_{mn}(R)(n\Omega^*-\omega^*)^2-\frac{(\Omega^*)^2}{{R_o}^2}\left[C_{rr}\frac{\partial^2 R_{mn}(R)}{\partial R^2}+C_{r\varphi}\frac{\partial R_{mn}(R)}{\partial R}-\right.$$

$$\left.\left.C_{\varphi\varphi}R_{mn}(R)\,n^2\right]\right\}a_{mn}a_{sn}\,R_{sn}(R)\,sin[n\varphi+(n\Omega^*-\omega^*)\tau]\,R\,dRd\varphi \qquad (9)$$

$$s=0,1,2,\dots,M$$

The only part of the function that depends on the angular coordinate, φ, is $\int_0^{2\pi} sin[n\varphi+(n\Omega^*-\omega^*)\tau]\,d\varphi$. This integral does not have to be equal to zero. So, Equation (9) can be rewritten in the following form;

$$\sum_{n=0}^{N}\sum_{m=0}^{M}\int_{\frac{R_i}{R_o}}^{1}\left\{\left(\frac{\partial^4 R_{mn}(R)}{\partial R^4}+\frac{2}{R}\frac{\partial^3 R_{mn}(R)}{\partial R^3}-\frac{1+2n^2}{R^2}\frac{\partial^2 R_{mn}(R)}{\partial R^2}+\frac{1+2n^2}{R^3}\frac{\partial R_{mn}(R)}{\partial R}+\right.\right.$$

$$\left.\frac{n^4-4n^2}{R^4}R_{mn}(R)\right)-R_{mn}(R)(n\Omega^*-\omega^*)^2-\frac{(\Omega^*)^2}{{R_o}^2}\left[C_{rr}\frac{\partial^2 R_{mn}(R)}{\partial R^2}+C_{r\varphi}\frac{\partial R_{mn}(R)}{\partial R}-\right.$$

$$\left.\left.C_{\varphi\varphi}R_{mn}(R)\,n^2\right]\right\}a_{mn}a_{sn}\,R_{sn}(R)R\,dR=0 \qquad (10)$$

For simplicity, $\phi^*_{smn}, \Gamma^*_{smn}, \lambda^*_{mn}$ and A^*_{smn} are described as follows;

$$\phi^*_{smn} = \int_{\frac{R_i}{R_o}}^{1} \left(\frac{\partial^4}{\partial R^4} + \frac{2}{R}\frac{\partial^3}{\partial R^3} - \frac{1+2n^2}{R^2}\frac{\partial^2}{\partial R^2} + \frac{1+2n^2}{R^3}\frac{\partial}{\partial R} + \frac{n^4-4n^2}{R^4} \right) R_{mn}(R)\, R_{sn}(R\,) R\, dR \; -$$

$$\int_{\frac{R_i}{R_o}}^{1} \frac{(\Omega^*)^2}{{R_o}^2} \left[C_{rr}\frac{\partial^2}{\partial R^2} + C_{r\varphi}\frac{\partial}{\partial R} - C_{\varphi\varphi}\, n^2 \right] R_{mn}(R)\, R_{sn}(R) R\, dR \qquad (11)$$

$$\Gamma^*_{smn} = \int_{\frac{R_i}{R_o}}^{1} R_{mn}(R)\, R_{sn}(R)\, R\, dR \qquad (12)$$

$$\lambda^*_{mn} = (n\Omega^* - \omega^*)^2 \qquad (13)$$

$$\mathrm{A}^*_{smn} = a_{mn} a_{sn} \qquad (14)$$

By using these abbreviations, Equation (10) can be rewritten as in Equation (15);

$$\sum_{n=0}^{N} \sum_{m=0}^{M} [\phi^*_{smn} - \lambda^*_{mn}\Gamma^*_{smn}]\, \mathrm{A}^*_{smn} = 0 \qquad (15)$$

To solve the unknown coefficients A^*_{smn}, the determinant of the coefficient matrix in Equation (15) must be zero. This will give the natural frequencies. Natural frequencies of spinning disks are expressed in Equation (16);

$$\omega^*{}_{mn1,2} = n\Omega^* \pm \lambda^*_{mn} \qquad (16)$$

As can be seen from Equation (16), the frequency has two varied values which are called forward and backward travelling waves except for $n = 0$ modes during rotation. The subscripts 1 and 2 correspond to the forward and backward travelling waves. Approximate function $R_{mn}(R)$ must be designated to get the frequency. To acquire $R_{mn}(R)$, five unknown constants, $X^1_{mn}, X^2_{mn}, X^3_{mn}, X^4_{mn}$ and X^5_{mn} are determined by using boundary and the normalization conditions.

Only uniform/axis-symmetric boundary conditions are considered in this study. It must be noted that there are also elastic, non-uniform and non-symmetric boundary conditions.

2.4 Analysed system

The effects of variations of radius ratio and rotational speeds on dimensionless frequencies are investigated. During the calculations, the values of nodal circles and nodal diameters are taken from 0 to 7 for nine different sets of boundary conditions and the behaviour of the disk is analysed under different rotational speeds varying from 2.29 to 34.30 and radius ratio changing from 0.1 to 0.5.

3. NUMERICAL AND EXPERIMENTAL ANALYSIS

In order to be able to validate the formulation, computational and experimental studies are performed. In the numerical approach, disks are modelled using S4R shell elements in ABAQUS environment and as a first step, the general static procedure is executed to model the influence of the rotational speed on the structure. Then, the frequency extraction procedure is executed to obtain the natural frequencies of the disk.

The stress and normalisation conditions considered can be described in Table 1.

Table 1. The stress and normalisation conditions for different boundary conditions.

Boundary Conditions	The stress coefficients	Normalization Conditions
C-C S-C C-S S-S	$C_{rr} = \frac{1}{8R^2}\left[(1+\nu)\left({R_i}^2+{R_o}^2\right)R^2+(1-\nu){R_i}^2-(3+\nu)R^4{R_o}^2\right]$ $C_{r\varphi} = \frac{1}{8R^3}\left[(1+\nu)\left({R_i}^2+{R_o}^2\right)R^2-(1-\nu){R_i}^2-3(3+\nu)R^4{R_o}^2\right]$ $C_{\varphi\varphi} = \frac{1}{8R^4}\left[(1+\nu)\left({R_i}^2+{R_o}^2\right)R^2-(1-\nu){R_i}^2-(1+3\nu)R^4{R_o}^2\right]$	$R_{mn}\left(\frac{R_i}{R_o}+\frac{R_o-R_i}{2R_o(m+1)}(2m+1)\right)=1$
C-F S-F”	$C_{rr} = \frac{(1-\nu^2)(R^2-1){R_i}^4+(3+\nu)\left((1+\nu)R^2{R_o}^2+(1-\nu){R_i}^2\right){R_o}^2}{8\left[(1+\nu){R_o}^2+(1-\nu){R_i}^2\right]R^2} - \frac{3+\nu}{8}R^2{R_o}^2$ $C_{r\varphi} = \frac{(1-\nu^2)(R^2+1){R_i}^4+(3+\nu)\left((1+\nu)R^2{R_o}^2+(\nu-1){R_i}^2\right){R_o}^2}{8\left[(1+\nu){R_o}^2+(1-\nu){R_i}^2\right]R^3} - \frac{3(3+\nu)R\,{R_o}^2}{8}$	$R_{mn}(1)=1$

	$C_{\varphi\varphi}=\frac{1}{8R^4}\left[(1+\nu)\left({R_i}^2+{R_o}^2\right)R^2-(1-\nu){R_i}^2-(1+3\nu)\,R^4{R_o}^2\right]$	
(F-C) (F-S)"	$C_{rr}=\left[\frac{(1-\nu)\left((3+\nu){R_i}^2-(1+\nu){R_o}^2\right)}{8R^2\left[(1+\nu){R_i}^2+(1-\nu){R_o}^2\right]}+\frac{3+\nu}{8}\right]\left({R_i}^2-R^2\,{R_o}^2\right)$ $C_{r\varphi}=\frac{3+\nu}{8\,R}\left({R_i}^2-3R^2\,{R_o}^2\right)-\frac{(1-\nu)\left[(3+\nu){R_i}^2-(1+\nu){R_o}^2\right]}{8R^3\left[(1+\nu){R_i}^2+(1-\nu){R_o}^2\right]}\left(R^2{R_o}^2+{R_i}^2\right)$ $C_{\varphi\varphi}=\frac{1}{8\,R^2}\left((3+\nu){R_i}^2-(1+3\nu)R^2R_o\right)-\frac{(1-\nu)\left[(3+\nu){R_i}^2-(1+\nu){R_o}^2\right]}{8\,R^4\left[(1+\nu){R_i}^2+(1-\nu){R_o}^2\right]}\left(R^2{R_o}^2+{R_i}^2\right)$	$R_{mn}\left(\frac{R_i}{R_o}\right)=1$
F-F	$C_{rr}=\frac{3+\nu}{8R^2}\left[(R^2-1)\left({R_i}^2-R^2{R_o}^2\right)\right]$ $C_{r\varphi}=\frac{3+\nu}{8R^3}\left[(R^2-1)\left({R_i}^2-R^2{R_o}^2\right)-2R^4{R_o}^2\right]$ $C_{\varphi\varphi}=\frac{1}{8\,R^4}\left[(3+\nu)(R^2-1){R_i}^2+{R_o}^2R^2-(1+3\nu)\,R^4{R_o}^2\right]$	$R_{mn}\left(\frac{R_i}{R_o}\right)=1$

As experimental validation, the rotating disk of the Seagate Barracuda ST2000DM001 hard disk driver is analysed. The outer and inner diameters of the disk are 95 mm and 32.5 mm, respectively and the thickness is 1.3 mm. Although the standard operating speed of the concerned HDD is 7200 rpm, using an electronic speed controller, variable rotational speed values can be obtained. In here, the disk is rotated at 0-2500-5000-7500 rpms. The speed of the disk is controlled via an accelerometer which is glued onto the casing. Due to the rotating nature of the structure, the vibration response is obtained using Polytec CLV- 2534 Compact Laser Doppler Vibrometer.

4. RESULTS AND DISCUSSION

Although both the nodal circle *m* and nodal diameter *n* values are taken from 0 to 7 in the analyses, the results of only four modes for each set of boundary conditions are presented in this study. For the mode shapes (*m,n*) notation is used.

For each boundary condition, the dimensionless frequencies obtained by the analytical method are compared with those of the FEM in Tables 2-10 for various dimensionless rotational speeds and the radius ratio.

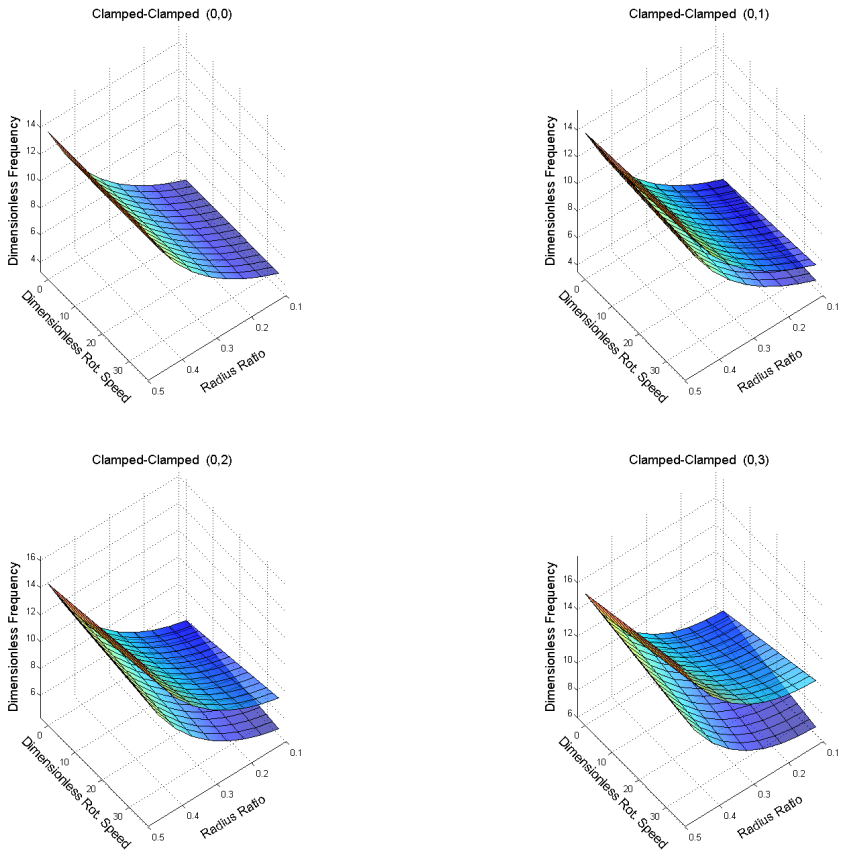
The results of the clamped-clamped disk are given in Table 2 and Figure 2. Here, the abbreviations FTW and BTW refer to the forward travelling wave and the backward travelling wave, respectively. For clamped-clamped boundary condition, the first thing to be pointed out is the insensitivity of the rotational speed, in other words, the natural frequencies do not change noticeably with varying rotational speed (Figure 2). This can be explained by the existence of both tensile and compressive stresses in the disk. As it is well known, tensile stress usually stiffens the structures whereas the compressive one softens. The co-existing stresses reduce the effects of each other in total so the insensitivity is observed.

Table 2. FEM and analytical solution comparisons for C-C boundary condition.

Radius Ratio	Dimensionless Rotational Speed	Wave Type	Dimensionless Frequency							
			(0,0)		(0,1)		(1,0)		(1,1)	
			FEM	This work	FEM	This work	FEM	This work	FEM	This work
0.1	2.29	FTW	4.30	4.34	4.59	4.64	11.78	11.99	12.31	12.55
		BTW	4.30	4.34	4.51	4.56	11.78	11.99	12.23	12.47
	34.30	FTW	4.30	4.33	5.13	5.18	11.79	12.01	12.86	13.10
		BTW	4.30	4.33	3.99	4.03	11.79	12.01	11.72	11.96
0.2	2.29	FTW	5.45	5.51	5.72	5.78	14.91	15.23	15.33	15.67
		BTW	5.45	5.51	5.64	5.71	14.91	15.23	15.26	15.60
	34.30	FTW	5.45	5.50	6.26	6.32	14.92	15.24	15.88	16.22
		BTW	5.45	5.50	5.11	5.17	14.92	15.24	14.74	15.08

0.3	2.29	FTW	7.13	7.21	7.36	7.46	19.42	19.95	19.76	20.30
		BTW	7.13	7.21	7.29	7.38	19.42	19.95	19.68	20.23
	34.30	FTW	7.12	7.21	7.90	7.99	19.43	19.95	20.30	20.85
		BTW	7.12	7.21	6.75	6.85	19.43	19.95	19.16	19.70
0.4	2.29	FTW	9.68	9.84	9.89	10.06	26.25	27.19	26.54	27.49
		BTW	9.68	9.84	9.82	9.98	26.25	27.19	26.46	27.42
	34.30	FTW	9.68	9.84	10.43	10.59	26.26	27.20	27.08	28.03
		BTW	9.68	9.84	9.28	9.45	26.26	27.20	25.93	26.89
0.5	2.29	FTW	13.88	14.20	14.07	14.39	37.41	39.19	37.65	39.45
		BTW	13.88	14.20	13.99	14.32	37.41	39.19	37.57	39.38
	34.30	FTW	13.88	14.20	14.60	14.93	37.41	39.20	38.19	39.99
		BTW	13.88	14.20	13.46	13.78	37.41	39.20	37.04	38.85

While n increases and radius ratio increases, the dimensionless frequency increases as well.



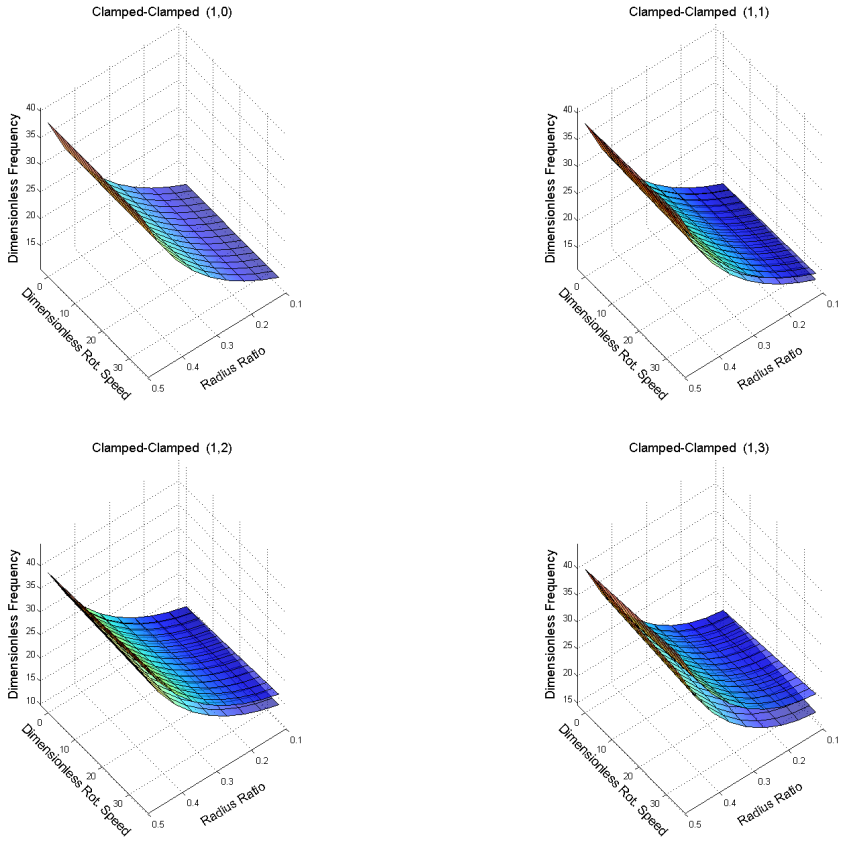


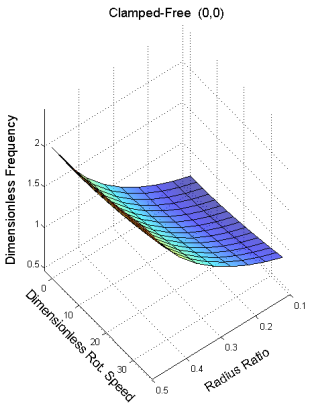
Figure 2. Variation of dimensionless frequencies for C-C.

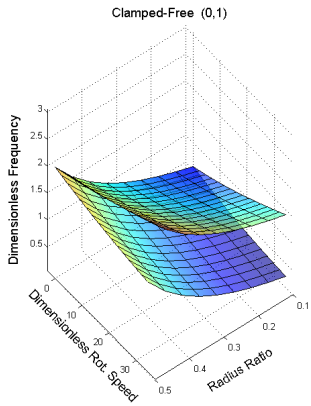
The clamped-free disk, are presented in Table 3 and Figure 3. The frequency of a clamped-free disk is affected considerably by both the radius ratio and the rotational speed (Figure 3). If nodal circle m and the nodal diameter n increase, the effects of the rotational speed and the radius ratio on the frequency becomes more significant as it is expected.

Table 3. FEM and analytical solution comparisons for C-F boundary condition.

Radius Ratio	Dimensionless Rotational Speed	Wave Type	Dimensionless Frequency							
			(0,0)		(0,1)		(1,0)		(1,1)	
			FEM	This work	FEM	This work	FEM	This work	FEM	This work
0.1	2.29	FTW	0.68	0.68	0.59	0.59	4.00	4.03	4.41	4.45
		BTW	0.68	0.68	0.51	0.52	4.00	4.03	4.33	4.37
	34.30	FTW	0.83	0.83	1.39	1.39	4.22	4.25	5.19	5.23
		BTW	0.83	0.83	0.24	0.25	4.22	4.25	4.04	4.08

0.2	2.29	FTW	0.83	0.83	0.80	0.81	5.11	5.15	5.49	5.54
		BTW	0.83	0.83	0.73	0.73	5.11	5.15	5.41	5.47
	34.30	FTW	0.99	0.99	1.57	1.57	5.33	5.37	6.25	6.30
		BTW	0.99	0.99	0.43	0.43	5.33	5.37	5.11	5.16
0.3	2.29	FTW	1.07	1.07	1.08	1.08	6.73	6.80	7.07	7.15
		BTW	1.07	1.07	1.00	1.01	6.73	6.80	7.00	7.08
	34.30	FTW	1.24	1.24	1.83	1.83	6.94	7.01	7.82	7.90
		BTW	1.24	1.24	0.68	0.69	6.94	7.01	6.67	6.75
0.4	2.29	FTW	1.44	1.44	1.49	1.49	9.22	9.34	9.53	9.66
		BTW	1.44	1.44	1.41	1.42	9.22	9.34	9.45	9.58
	34.30	FTW	1.62	1.62	2.22	2.22	9.41	9.53	10.25	10.39
		BTW	1.62	1.62	1.07	1.08	9.41	9.53	9.11	9.24
0.5	2.29	FTW	2.08	2.08	2.15	2.16	13.31	13.55	13.60	13.85
		BTW	2.08	2.08	2.07	2.08	13.31	13.55	13.52	13.78
	34.30	FTW	2.24	2.25	2.86	2.87	13.48	13.72	14.30	14.56
		BTW	2.24	2.25	1.71	1.72	13.48	13.72	13.16	13.41





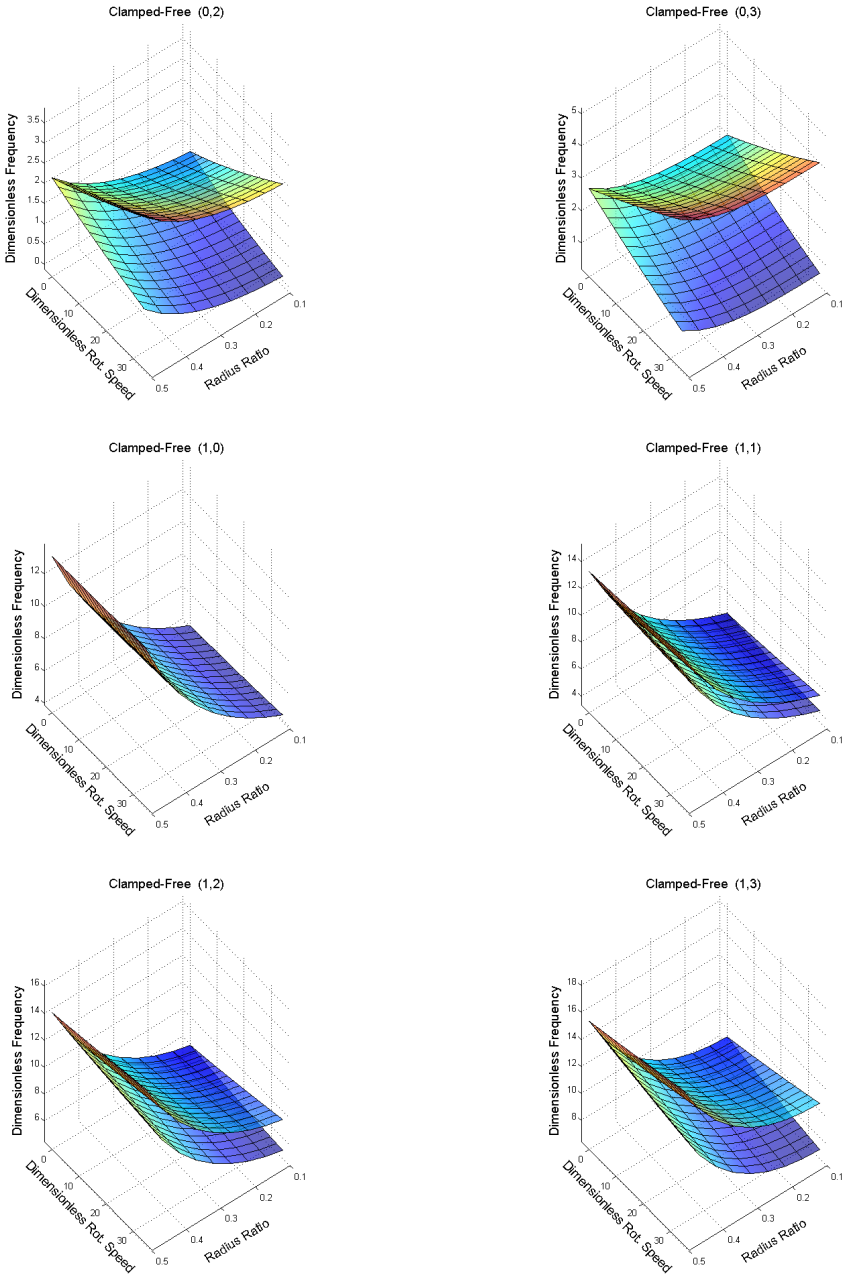
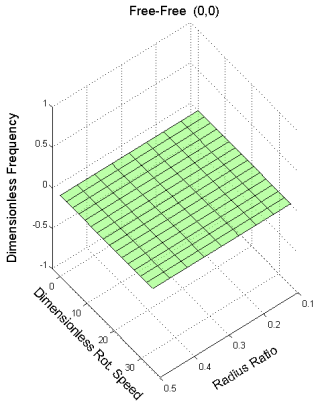


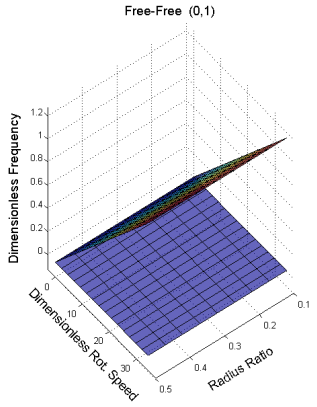
Figure 3. Variation of dimensionless frequencies for C-F.

For m=0, with an increasing radius ratio, if n increases, the growth rate in frequency diminishes. For higher n values, while the radius ratio increases, the frequency grows slowly first, then the growth takes up. Due to the dominant tensile stresses in the disk, the structure shows stiffening behaviour. The results of the disk with F-F boundary condition are given in Table 4 and Figure 4 and.

Table 4. FEM and analytical solution comparisons for F-F boundary condition.

Radius Ratio	Dimensionless Rotational Speed	Wave Type	Dimensionless Frequency							
			(0,2)		(0,3)		(1,0)		(1,1)	
			FEM	This work	FEM	This work	FEM	This work	FEM	This work
0.1	2.29	FTW	0.90	0.91	2.05	2.06	1.40	1.41	3.28	3.31
		BTW	0.75	0.75	1.82	1.83	1.40	1.41	3.20	3.23
	34.30	FTW	2.35	2.36	3.97	3.98	1.76	1.76	4.11	4.14
		BTW	0.07	0.07	0.54	0.55	1.76	1.76	2.97	3.00
0.2	2.29	FTW	0.88	0.88	2.05	2.05	1.34	1.35	3.14	3.17
		BTW	0.73	0.73	1.82	1.83	1.34	1.35	3.07	3.10
	34.30	FTW	2.36	2.36	4.00	4.00	1.72	1.72	3.98	4.01
		BTW	0.07	0.08	0.57	0.57	1.72	1.72	2.84	2.87
0.3	2.29	FTW	0.84	0.85	2.02	2.03	1.32	1.33	2.89	2.93
		BTW	0.69	0.69	1.80	1.81	1.32	1.33	2.81	2.85
	34.30	FTW	2.37	2.37	4.02	4.03	1.70	1.70	3.74	3.78
		BTW	0.08	0.09	0.59	0.60	1.70	1.70	2.60	2.63
0.4	2.29	FTW	0.80	0.80	1.98	1.99	1.36	1.36	2.71	2.75
		BTW	0.64	0.65	1.75	1.76	1.36	1.36	2.63	2.67
	34.30	FTW	2.38	2.38	4.04	4.05	1.72	1.73	3.55	3.59
		BTW	0.09	0.10	0.61	0.62	1.72	1.73	2.41	2.45
0.5	2.29	FTW	0.75	0.75	1.90	1.91	1.47	1.47	2.69	2.73
		BTW	0.59	0.60	1.67	1.68	1.47	1.47	2.61	2.66
	34.30	FTW	2.39	2.39	4.04	4.05	1.81	1.81	3.51	3.56
		BTW	0.10	0.10	0.61	0.62	1.81	1.81	2.37	2.41





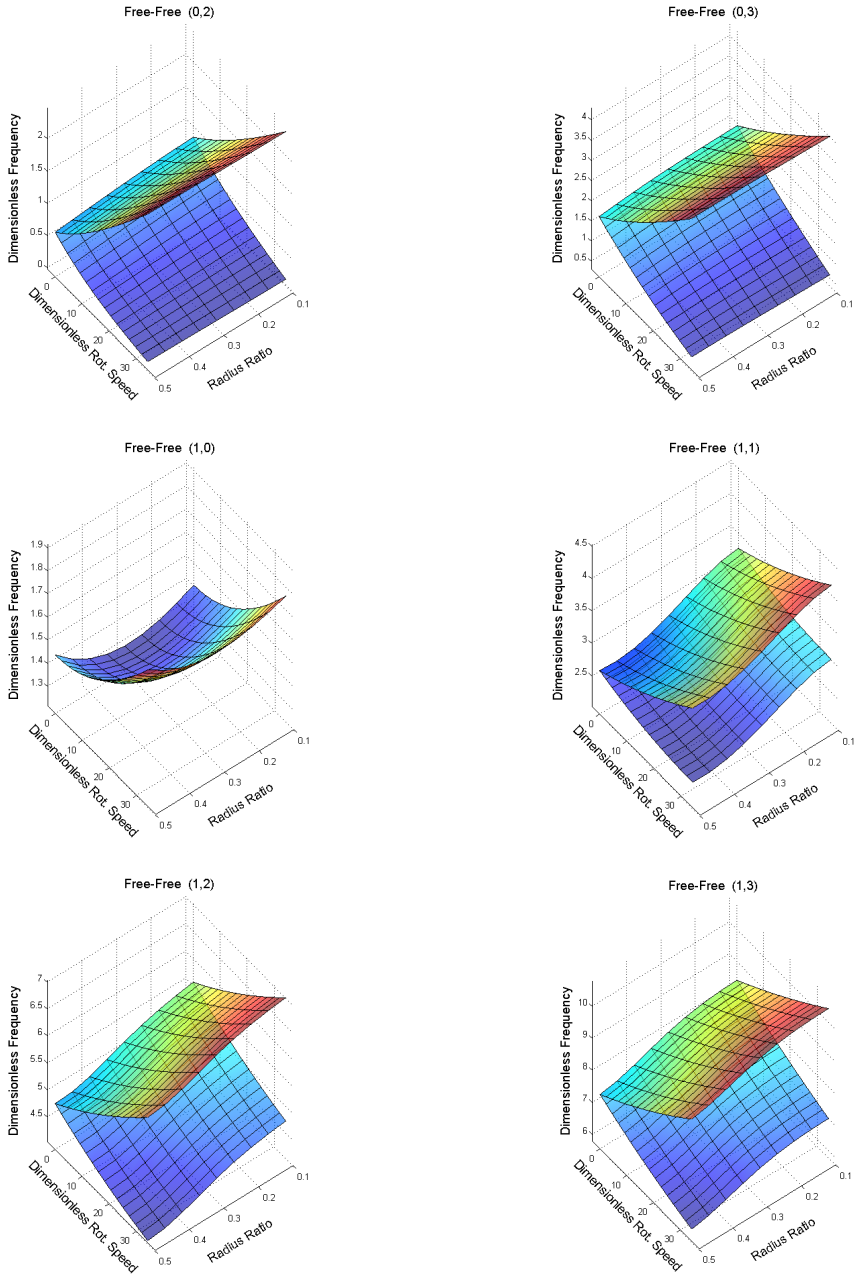


Figure 4. Variation of dimensionless frequencies for F-F.

The modes (0,0) and (0,1) of the free-free disk are rigid body modes due to having no motion constraints (Figure 4). So, in Table 4, the results of (0,2) and (0,3) are given. The effect of the rotational speed on the frequency is more significant than it is in the other boundary conditions. All modes of the free disk are affected considerably by the rotational speed. The dependence of the natural frequencies on rotational speed is not linear unlike most of the other sets of boundary conditions. The stiffening behaviour

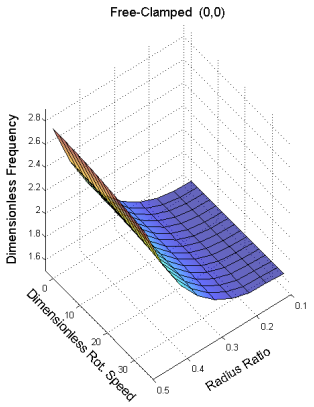
is as obvious as the clamped-free disk. The underlying reason is the dominant tensile stresses that are caused by the centrifugal body forces. While the radius ratio increases, the frequency decreases (except mode (1,0)) unlike most of the other sets of boundary conditions. The modes where m=0 are insensitive to changes in radius ratio, whereas the modes where m>0 are affected significantly by the radius ratio. In mode (1,0), a local minimum exists for each curve fibre extracted from this surface for a fixed value of rotational speed. This is also valid for curves for a fixed radius ratio as well. While the radius ratio increases, the change in the frequency becomes less for each rotational speed.

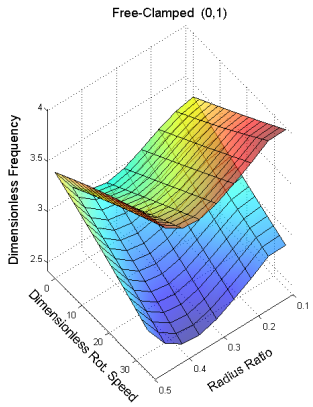
For the disk with F-C boundary condition, the change of the frequency with the radius ratio and rotation speed is given in Table 5 and Figure 5. The disk displays a significant softening due to the compressive stresses that influence the behaviour of the disk. The frequency decreases slightly when the rotational speed increases. The radius ratio also has a significant impact on the dynamics of the free-clamped disk. For the mode with m=0 and n=1, the frequency has a minimum value for each rotational speed. The minimum is between the radius ratio of 0.3 and 0.4. The dimensionless frequency values keep decreasing until this value of radius ratio, then, it increases monotonically towards the radius ratio of 0.5. Similar behaviour can be observed in the mode (0,2), but, for all other modes with m=0, all dimensionless frequency values decrease while the radius ratio increases. For higher m and n values, the decrease in the frequency increases by increasing the rotational speed.

Table 5. FEM and analytical solution comparisons for F-C boundary condition.

Radius Ratio	Dimensionless Rotational Speed	Wave Type	Dimensionless Frequency							
			(0,0)		(0,1)		(1,0)		(1,1)	
			FEM	This work	FEM	This work	FEM	This work	FEM	This work

0.1	2.29	FTW	1.61	1.61	3.39	3.41	6.22	6.27	9.45	9.59
		BTW	1.61	1.61	3.32	3.33	6.22	6.27	9.37	9.51
	34.30	FTW	1.62	1.62	3.95	3.97	6.26	6.31	10.02	10.16
		BTW	1.62	1.62	2.81	2.83	6.26	6.31	8.88	9.01
0.2	2.29	FTW	1.64	1.65	3.27	3.30	6.76	6.81	8.86	9.04
		BTW	1.64	1.65	3.19	3.22	6.76	6.81	8.78	8.96
	34.30	FTW	1.63	1.63	3.82	3.85	6.76	6.82	9.42	9.59
		BTW	1.63	1.63	2.68	2.71	6.76	6.82	8.27	8.45
0.3	2.29	FTW	1.80	1.80	3.09	3.12	8.12	8.20	9.31	9.48
		BTW	1.80	1.80	3.01	3.05	8.12	8.20	9.24	9.41
	34.30	FTW	1.76	1.76	3.62	3.66	8.08	8.16	9.83	10.00
		BTW	1.76	1.76	2.48	2.52	8.08	8.16	8.69	8.85
0.4	2.29	FTW	2.14	2.15	3.08	3.12	10.51	10.65	11.27	11.47
		BTW	2.14	2.15	3.01	3.05	10.51	10.65	11.19	11.39
	34.30	FTW	2.07	2.07	3.59	3.62	10.44	10.58	11.74	11.94
		BTW	2.07	2.07	2.44	2.48	10.44	10.58	10.60	10.80
0.5	2.29	FTW	2.79	2.80	3.47	3.50	14.62	14.89	15.16	15.48
		BTW	2.79	2.80	3.39	3.43	14.62	14.89	15.08	15.40
	34.30	FTW	2.69	2.70	3.93	3.97	14.54	14.81	15.61	15.93
		BTW	2.69	2.70	2.79	2.83	14.54	14.81	14.47	14.78





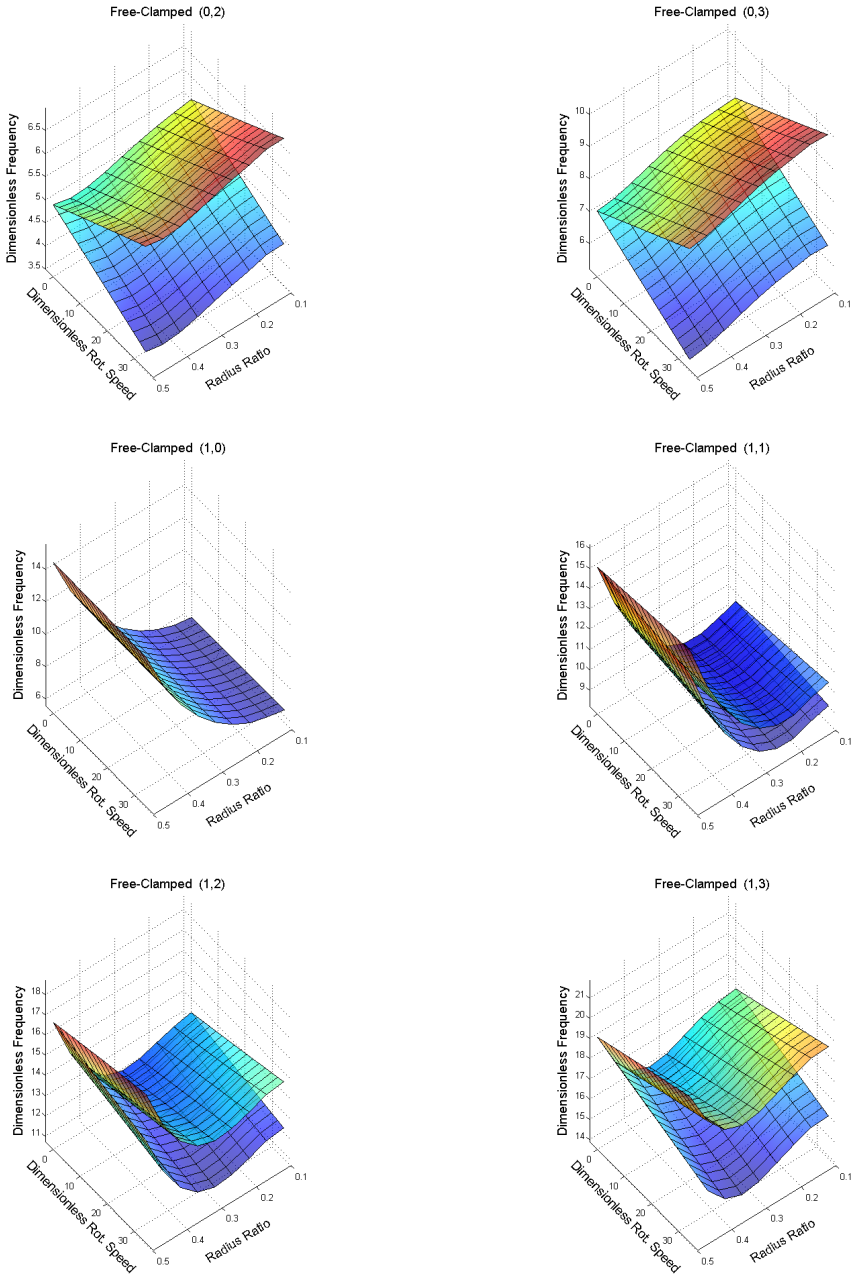


Figure 5. Variation of dimensionless frequencies for F-C.

On one hand, considering that the stress distributions are exactly the same for simple supports and clamps, on the other hand, as described, the simple supports impose less restriction to the system than clamps do. Therefore, one can predict that the mechanical behaviour of a rotating disk with simple supports is more compliant compared to a clamped disk and consequently the natural frequencies are slightly lower than the cases where simple support is replaced with a clamp. So, it is obtained as predicted.

Table 6. FEM and analytical solution comparisons for S-S boundary condition.

Radius Ratio	Dimensionless Rotational Speed	Wave Type	Dimensionless Frequency							
			(0,0)		(0,1)		(1,0)		(1,1)	
			FEM	This work	FEM	This work	FEM	This work	FEM	This work
0.1	2.29	FTW	2.29	2.30	2.66	2.70	8.15	8.22	8.87	9.02
		BTW	2.29	2.30	2.58	2.63	8.15	8.22	8.80	8.94
	34.30	FTW	2.23	2.23	3.15	3.20	8.15	8.21	9.41	9.55
		BTW	2.23	2.23	2.01	2.05	8.15	8.21	8.26	8.41
0.2	2.29	FTW	2.65	2.66	3.06	3.09	9.98	10.07	10.57	10.70
		BTW	2.65	2.66	2.98	3.02	9.98	10.07	10.49	10.63
	34.30	FTW	2.61	2.61	3.56	3.59	9.98	10.07	11.10	11.24
		BTW	2.61	2.61	2.41	2.45	9.98	10.07	9.96	10.09
0.3	2.29	FTW	3.34	3.35	3.71	3.74	12.85	12.99	13.31	13.49
		BTW	3.34	3.35	3.64	3.67	12.85	12.99	13.24	13.41
	34.30	FTW	3.30	3.31	4.22	4.25	12.85	12.99	13.85	14.03
		BTW	3.30	3.31	3.07	3.10	12.85	12.99	12.71	12.88
0.4	2.29	FTW	4.45	4.47	4.79	4.82	17.32	17.58	17.70	17.99
		BTW	4.45	4.47	4.71	4.75	17.32	17.58	17.63	17.91
	34.30	FTW	4.43	4.44	5.30	5.33	17.33	17.58	18.24	18.52
		BTW	4.43	4.44	4.15	4.19	17.33	17.58	17.09	17.38
0.5	2.29	FTW	6.33	6.36	6.63	6.68	24.74	25.23	25.06	25.57
		BTW	6.33	6.36	6.55	6.61	24.74	25.23	24.98	25.50
	34.30	FTW	6.31	6.35	7.15	7.20	24.74	25.23	25.59	26.11
		BTW	6.31	6.35	6.00	6.05	24.74	25.23	24.45	24.97

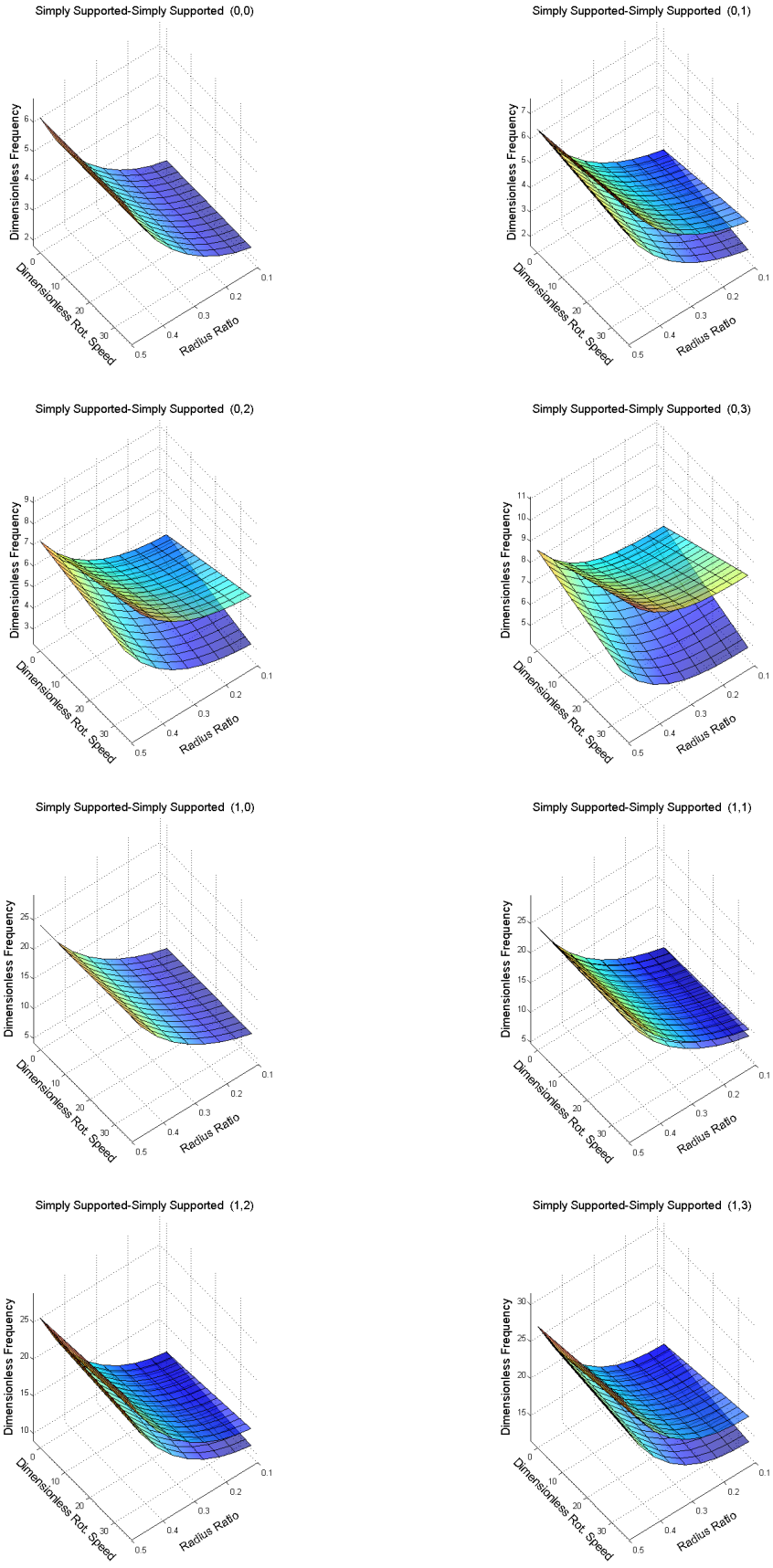


Figure 6. Variation of dimensionless frequencies for S-S.

Compared to the C-C disk, the S-S, S-C and C-S disks have lower natural frequency values but a similar variation trend of the natural frequency with changing rotational speed and radius ratio as presented in Tables 6-8 and Figures 6-8.

Table 7. Results of FE and analytical methods for S-C boundary condition.

Radius Ratio	Dimensionless Rotational Speed	Wave Type	Dimensionless Frequency							
			(0,0)		(0,1)		(1,0)		(1,1)	
			FEM	This work	FEM	This work	FEM	This work	FEM	This work
0.1	2.29	FTW	3.57	3.59	3.98	4.05	10.29	10.41	11.05	11.26
		BTW	3.57	3.59	3.91	3.97	10.29	10.41	10.97	11.19
	34.30	FTW	3.58	3.60	4.54	4.60	10.32	10.44	11.61	11.83
		BTW	3.58	3.60	3.39	3.46	10.32	10.44	10.47	10.68
0.2	2.29	FTW	4.21	4.23	4.62	4.68	12.64	12.82	13.22	13.46
		BTW	4.21	4.23	4.55	4.60	12.64	12.82	13.15	13.38
	34.30	FTW	4.23	4.25	5.18	5.23	12.67	12.85	13.79	14.02
		BTW	4.23	4.25	4.04	4.09	12.67	12.85	12.65	12.88
0.3	2.29	FTW	5.32	5.35	5.68	5.73	16.26	16.56	16.71	17.05
		BTW	5.32	5.35	5.60	5.66	16.26	16.56	16.64	16.97
	34.30	FTW	5.34	5.38	6.24	6.29	16.30	16.59	17.28	17.61
		BTW	5.34	5.38	5.09	5.15	16.30	16.59	16.14	16.47
0.4	2.29	FTW	7.08	7.15	7.39	7.47	21.88	22.40	22.23	22.79
		BTW	7.08	7.15	7.31	7.40	21.88	22.40	22.16	22.71
	34.30	FTW	7.11	7.17	7.95	8.03	21.90	22.43	22.79	23.35
		BTW	7.11	7.17	6.81	6.89	21.90	22.43	21.65	22.21
0.5	2.29	FTW	10.03	10.16	10.29	10.44	31.12	32.13	31.41	32.45
		BTW	10.03	10.16	10.22	10.36	31.12	32.13	31.33	32.37
	34.30	FTW	10.06	10.19	10.85	11.00	31.14	32.15	31.97	33.00
		BTW	10.06	10.19	9.71	9.85	31.14	32.15	30.82	31.86

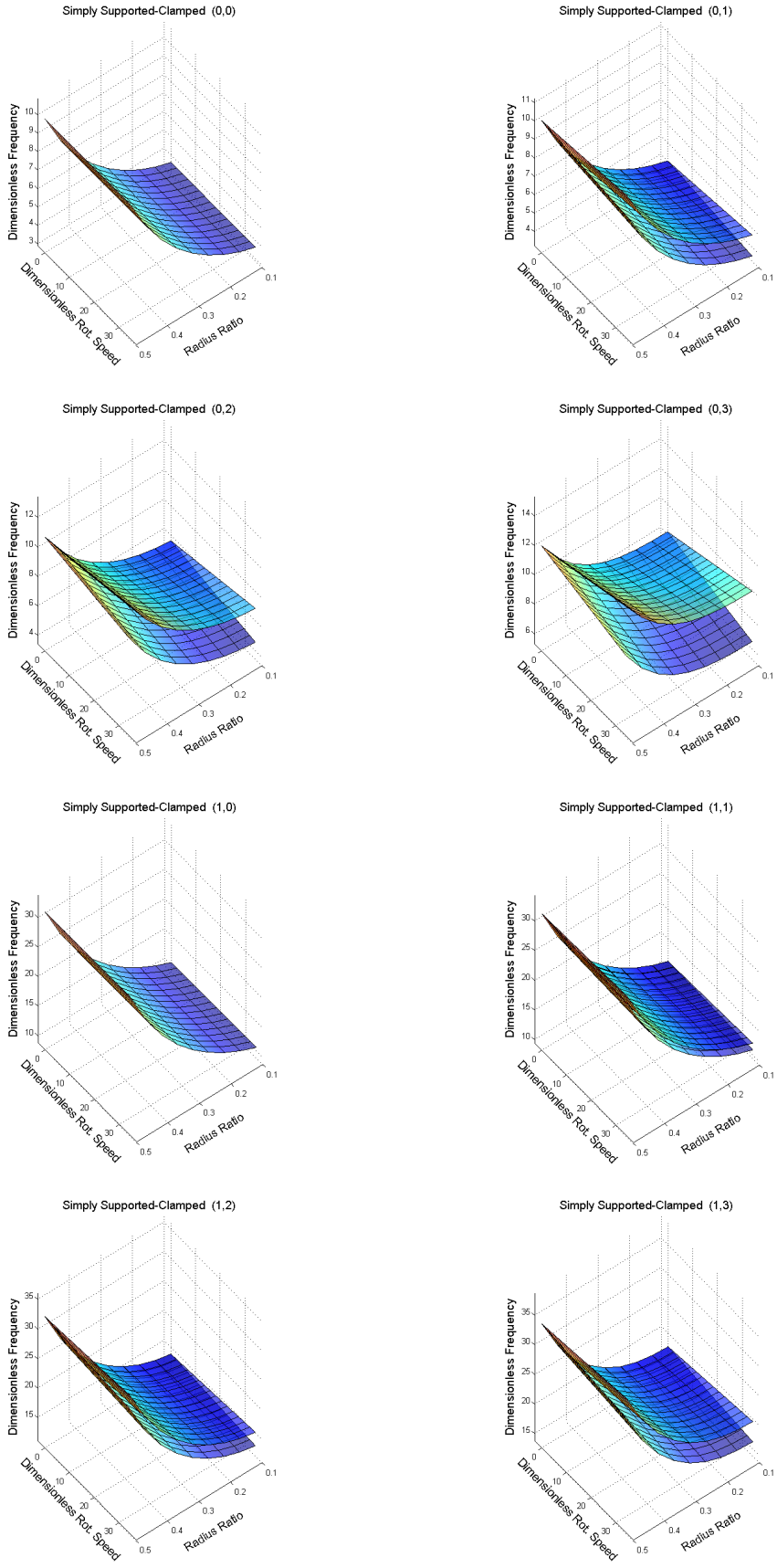


Figure 7. Variation of dimensionless frequencies for S-C.

Increasing rotational speed increases the dominant compressive stresses in the disk and that leads to a softening effect. For the C-S disk, dimensionless frequency values decrease for the increasing rotational speed in modes (0,0) and (0,1) in Table 8.

Table 8. FEM and analytical solution comparisons for C-S boundary condition.

Radius Ratio	Dimensionless Rotational Speed	Wave Type	Dimensionless Frequency							
			(0,0)		(0,1)		(1,0)		(1,1)	
			FEM	This work	FEM	This work	FEM	This work	FEM	This work
0.1	2.29	FTW	2.82	2.84	3.11	3.13	9.46	9.57	9.97	10.11
		BTW	2.82	2.84	3.03	3.05	9.46	9.57	9.89	10.03
	34.30	FTW	2.75	2.77	3.59	3.61	9.44	9.55	10.49	10.63
		BTW	2.75	2.77	2.44	2.47	9.44	9.55	9.34	9.48
0.2	2.29	FTW	3.60	3.62	3.88	3.91	12.01	12.18	12.43	12.62
		BTW	3.60	3.62	3.70	3.83	12.01	12.18	12.35	12.55
	34.30	FTW	3.54	3.56	4.36	4.39	11.99	12.16	12.95	13.14
		BTW	3.54	3.56	3.21	3.24	11.99	12.16	11.80	11.99
0.3	2.29	FTW	4.74	4.78	5.00	5.04	15.69	15.98	16.04	16.35
		BTW	4.74	4.78	4.93	4.97	15.69	15.98	15.97	16.27
	34.30	FTW	4.69	4.72	5.48	5.52	15.67	15.96	16.56	16.86
		BTW	4.69	4.72	4.34	4.38	15.67	15.96	15.41	15.72
0.4	2.29	FTW	6.50	6.56	6.74	6.81	21.31	21.83	21.61	22.14
		BTW	6.50	6.56	6.66	6.73	21.31	21.83	21.53	22.07
	34.30	FTW	6.45	6.51	7.22	7.29	21.29	21.81	22.12	22.66
		BTW	6.45	6.51	6.08	6.15	21.29	21.81	20.98	21.51
0.5	2.29	FTW	9.40	9.53	9.62	9.75	30.52	31.52	30.78	31.79
		BTW	9.40	9.53	9.54	9.68	30.52	31.52	30.70	31.72
	34.30	FTW	9.36	9.49	10.11	10.24	30.50	31.50	31.29	32.31
		BTW	9.36	9.49	8.97	9.10	30.50	31.50	30.15	31.16

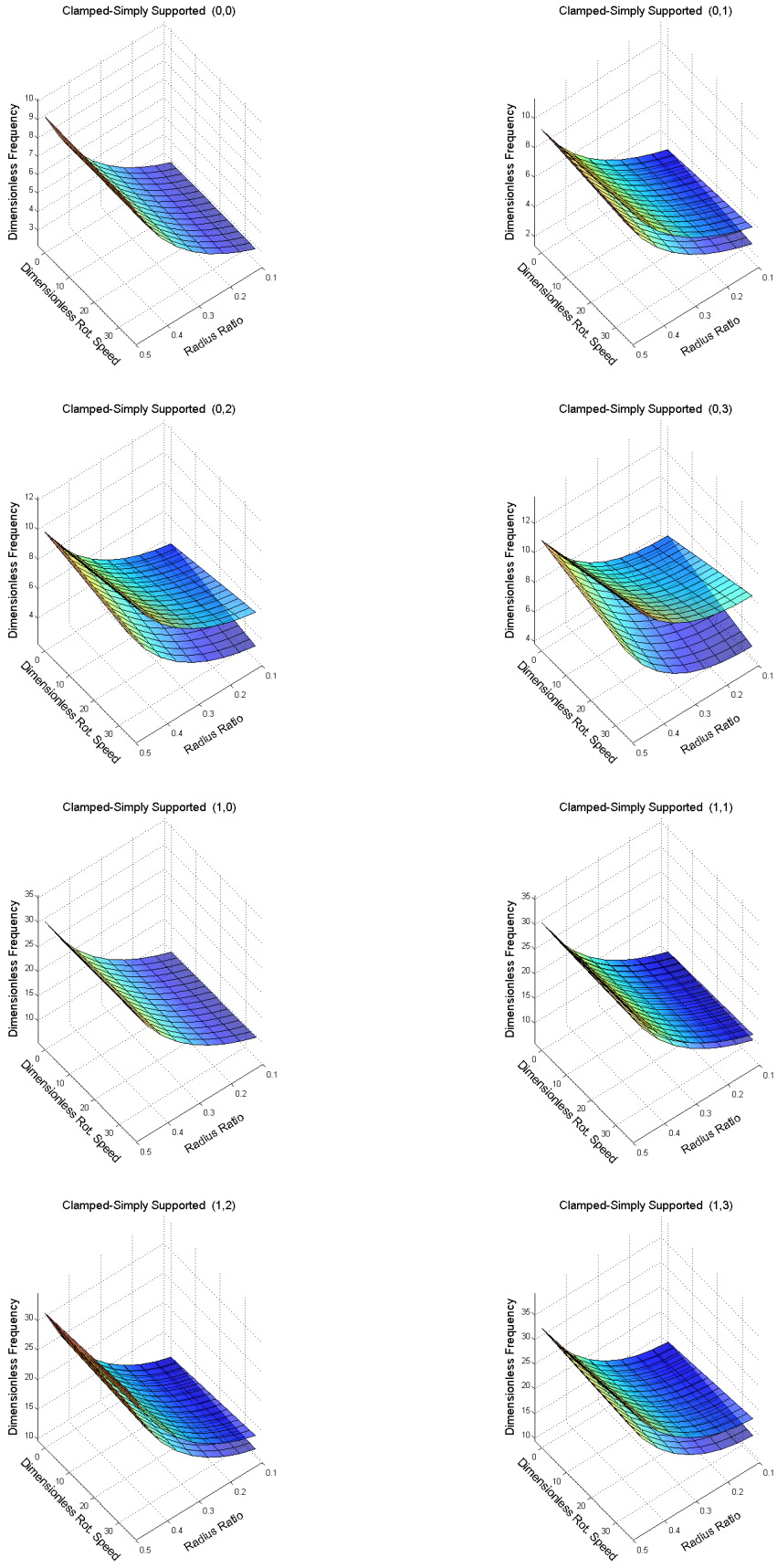


Figure 8. Variation of dimensionless frequencies for C-S.

Table 9. FEM and analytical solution comparisons for F-S boundary condition.

Radius Ratio	Dimensionless Rotational Speed	Wave Type	Dimensionless Frequency							
			(0,0)		(0,1)		(1,0)		(1,1)	
			FEM	This work	FEM	This work	FEM	This work	FEM	This work
0.1	2.29	FTW	0.78	0.78	2.24	2.25	4.66	4.67	7.60	7.68
		BTW	0.78	0.78	2.17	2.17	4.66	4.67	7.53	7.60
	34.30	FTW	0.66	0.66	2.74	2.75	4.66	4.68	8.14	8.22
		BTW	0.66	0.66	1.60	1.61	4.66	4.68	7.00	7.07
0.2	2.29	FTW	0.75	0.75	2.19	2.20	4.95	4.97	7.11	7.23
		BTW	0.75	0.75	2.11	2.12	4.95	4.97	7.04	7.15
	34.30	FTW	0.60	0.60	2.67	2.68	4.92	4.94	7.64	7.75
		BTW	0.60	0.60	1.53	1.54	4.92	4.94	6.50	6.61
0.3	2.29	FTW	0.74	0.74	2.05	2.07	5.84	5.87	7.17	7.28
		BTW	0.74	0.74	1.97	1.99	5.84	5.87	7.10	7.20
	34.30	FTW	0.50	0.50	2.52	2.54	5.76	5.78	7.66	7.76
		BTW	0.50	0.50	1.38	1.39	5.76	5.78	6.51	6.62
0.4	2.29	FTW	0.75	0.75	1.91	1.93	7.48	7.52	8.35	8.45
		BTW	0.75	0.75	1.83	1.85	7.48	7.52	8.27	8.37
	34.30	FTW	0.37	0.37	2.34	2.36	7.36	7.40	8.78	8.88
		BTW	0.37	0.37	1.19	1.22	7.36	7.40	7.64	7.74
0.5	2.29	FTW	0.80	0.80	1.83	1.86	10.36	10.45	10.98	11.11
		BTW	0.80	0.80	1.76	1.78	10.36	10.45	10.91	11.04
	34.30	FTW	0.15	0.15	2.20	2.23	10.22	10.30	11.38	11.51
		BTW	0.15	0.15	1.05	1.08	10.22	10.30	10.24	10.37

F-S and S-F boundary condition combinations exhibit softer behaviour than the combinations where simple supports are replaced with clamps. These results are displayed in Figures 9, 10, and Tables 9 and 10. For example, while the maximum dimensionless frequency value is 15.93 for the mode (1,1) of the F-C disk given in Table 5, this value is 11.51 in the same mode of the F-S disk as shown in Table 9.

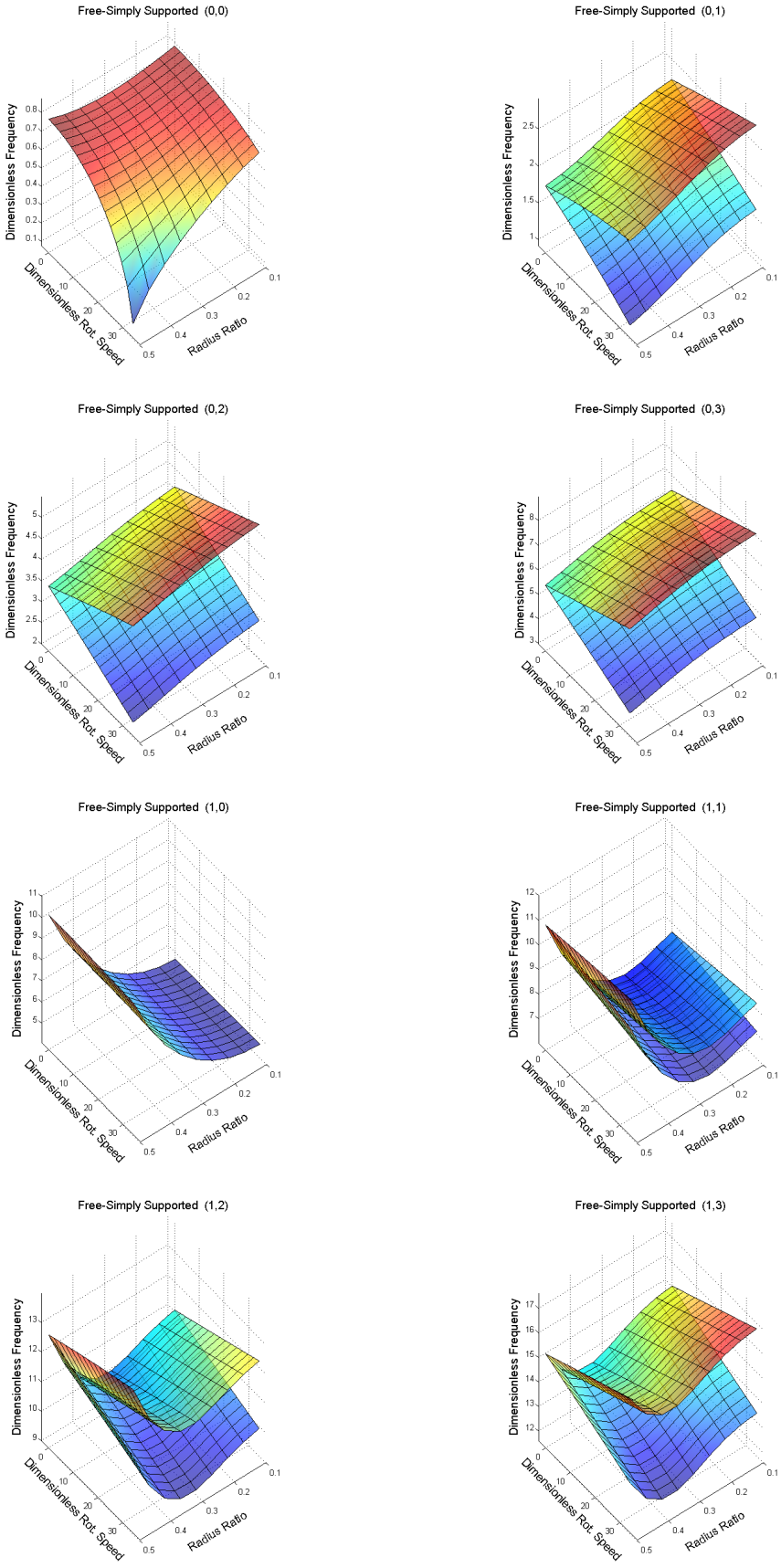


Figure 9. Variation of dimensionless frequencies for F-S.

The characteristics of the frequencies of F-C and F-S disks are almost the same except for the mode (0,0) (Figures 5 and 9). The same also is observed for C-F and S-F disks from Figures 3 and 10. For the mode (0,0), the rotational speed affects considerably the frequency for each radius ratio. In Figure 9, this effect is noticeably large for small radius ratios but it is significantly large for larger radius ratios. If the radius ratio increases, the frequency decreases remarkably for higher rotational speeds.

Table 10. FEM and analytical solution comparisons for S-F boundary condition.

Radius Ratio	Dimensionless Rotational Speed	Wave Type	Dimensionless Frequency							
			(0,0)		(0,1)		(1,0)		(1,1)	
			FEM	This work	FEM	This work	FEM	This work	FEM	This work
0.1	2.29	FTW	0.55	0.55	0.40	0.42	3.31	3.32	3.83	3.89
		BTW	0.55	0.55	0.33	0.35	3.31	3.32	3.76	3.82
	34.30	FTW	0.69	0.69	1.26	1.27	3.56	3.57	4.65	4.70
		BTW	0.69	0.69	0.12	0.13	3.56	3.57	3.50	3.56
0.2	2.29	FTW	0.53	0.53	0.48	0.49	3.93	3.94	4.45	4.49
		BTW	0.53	0.53	0.40	0.41	3.93	3.94	4.37	4.42
	34.30	FTW	0.72	0.72	1.33	1.34	4.21	4.22	5.26	5.30
		BTW	0.72	0.72	0.18	0.19	4.21	4.22	4.12	4.16
0.3	2.29	FTW	0.54	0.54	0.56	0.57	5.01	5.03	5.47	5.52
		BTW	0.54	0.54	0.48	0.49	5.01	5.03	5.40	5.44
	34.30	FTW	0.79	0.79	1.41	1.42	5.29	5.31	6.28	6.33
		BTW	0.79	0.79	0.27	0.28	5.29	5.31	5.14	5.18
0.4	2.29	FTW	0.58	0.58	0.65	0.66	6.74	6.77	7.14	7.20
		BTW	0.58	0.58	0.58	0.59	6.74	6.77	7.07	7.13
	34.30	FTW	0.90	0.90	1.53	1.54	7.01	7.04	7.94	8.00
		BTW	0.90	0.90	0.39	0.39	7.01	7.04	6.80	6.86
0.5	2.29	FTW	0.65	0.65	0.78	0.80	9.64	9.71	10.00	10.10
		BTW	0.65	0.65	0.71	0.72	9.64	9.71	9.92	10.02
	34.30	FTW	1.03	1.03	1.69	1.70	9.88	9.96	10.78	10.87
		BTW	1.03	1.03	0.55	0.56	9.88	9.96	9.63	9.73

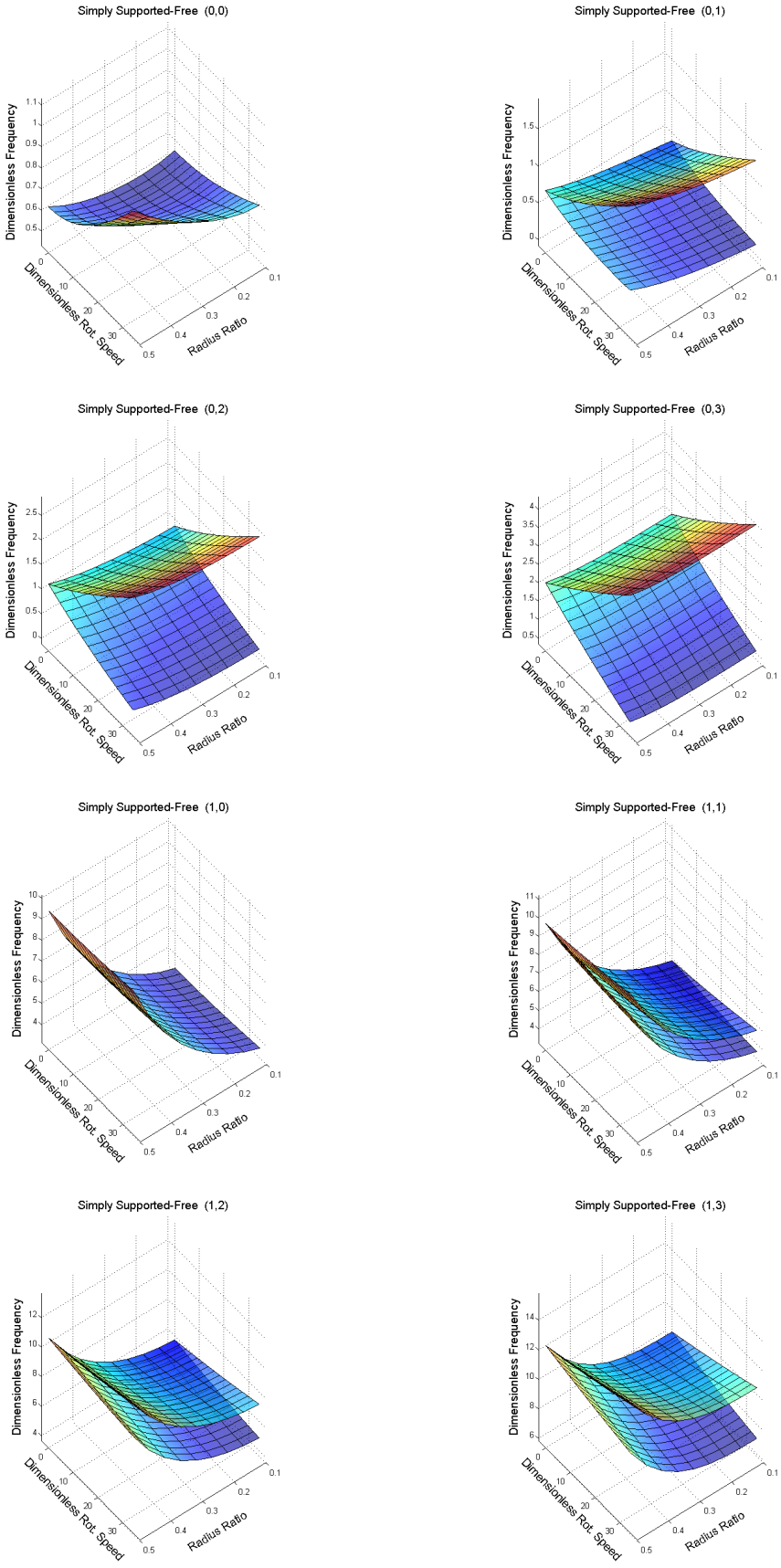


Figure 10. Variation of dimensionless frequencies for S-F.

For the stationary F-S disk, the frequency has a minimum around the radius ratio of 0.3-0.4. This minimum is preserved after the rotational speed increases.

For an S-F disk, the results of FEM and analytical methods are given in Table 10 and Figures 10. The characteristics of the frequency change against the rotational speed and the radius ratio is very similar to those of the C-F disk except for the mode (0,0), as can be seen easily from Figures 3 and 10. For the stationary S-F disk, the frequency has a minimum around the radius ratio of 0.2-0.3. This minimum moves to the radius ratio of 0.1 by increasing rotational speed. For smaller radius ratios, a minimum of the frequency is observed for specific rotational speed, but this disappears after higher radius ratios. When the rotational speed increases, the frequency slightly decreases first, then increases after a minimum for smaller radius ratios, and it increases gradually for higher radius ratios.

In practice, it should be stated that all the abovementioned explanations are valuable and can be helpful for those who study rotating annular disks. With the help of the detailed parametric study given above, one can select the “optimal” rotational speed-radius ratio pair for the need under certain boundary conditions. In addition, the role of boundary conditions on modal behaviour is explained through stress distributions. By considering stress distributions, it is believed that causes of hardening or softening of the structure and behavioural similarities between certain modes belong to different boundary conditions can be more understandable on a physical basis.

As it can be seen from all tables and figures, the results of the FEM and the analytical methods for all boundary conditions are in good agreement in both values and changes depending on the radius ratio and the rotational speed.

Apart from these, to show the advantages of the selected approximation function, a comparative study is conducted using the three-term polynomial by Huang

and Hsu (Huang and Hsu 1992). The 3-term approximate solution, only convenient for C-F boundary condition, assumption is taken and adapted into the formulation presented within this study. The rest of the sets of boundary conditions are not naturally satisfied and therefore, they cannot be handled using this approximate solution. Obtained results are compared with this study in Table 11.

Table 11. Analytical solution comparisons by using approximate function having three and 5-term for C-F boundary condition.

Radius Ratio	Dimensionless Rotational Speed	Wave Type	Dimensionless Frequency							
			(0,2)		(0,3)		(1,2)		(1,3)	
			3 terms	This work	3 terms	This work	3 terms	This work	3 terms	This work
0.2	2.29	FTW	1.09	1.09	2.09	2.09	6.75	6.75	8.91	8.91
		BTW	0.93	0.93	1.86	1.86	6.60	6.60	8.69	8.69
	34.30	FTW	2.47	2.47	3.98	3.98	8.06	8.06	10.76	10.76
		BTW	0.19	0.19	0.55	0.55	5.77	5.77	7.33	7.33
0.4	2.29	FTW	1.73	1.73	2.46	2.46	10.57	10.57	12.10	12.10
		BTW	1.57	1.57	2.23	2.23	10.42	10.42	11.87	11.87
	34.30	FTW	3.02	3.02	4.29	4.29	11.83	11.83	13.90	13.90
		BTW	0.73	0.73	0.86	0.86	9.54	9.54	10.47	10.47

When compared to approximate functions having three and five terms used, it is seen that obtained results are almost the same in Table 11. Therefore, the questions regarding the convergence of this formulation are also clarified. To emphasise, the strength of the formulation is the generalisability for all the classical, axisymmetric boundary conditions while their convergences are ensured.

Moreover, the data acquired from the experimental study conducted on the hard disk set-up is compiled in Table 12. The values in brackets are the dimensional values whereas the rest is nondimensionalised for the sake of consistency. The error margins are presented in percentage.

Table 12. Comparison study between analytical and experimental study for C-F boundary condition.

Rotational Speed	Studies	Wave type	Dimensionless Frequency					
			(0,0)	(0,1)	(0,2)	(0,3)	(0,4)	(0,5)
0 (0)	This Study	-	1.203	1.195	1.394	2.162	3.495	5.275
	Experimental		1.299 (1136)	1.092 (955)	1.409 (1232)	2.092 (1830)	3.441 (3009)	5.214 (4560)
	Error %		7.380	9.400	1.072	3.303	1.568	1.178
2.86 (2500)	This Study	FTW	1.204	1.244	1.491	2.306	3.687	5.515
	Experimental		1.307 (1143)	1.123 (982)	1.504 (1315)	2.239 (1958)	3.625 (3170)	5.447 (4764)
	Error %		7.846	10.774	0.850	3.017	1.714	1.247
	This Study	BTW	1.204	1.149	1.300	2.021	3.306	5.039
	Experimental		1.307 (1143)	1.030 (901)	1.307 (1143)	1.952 (1707)	3.237 (2831)	4.951 (4330)
	Error %		7.846	11.483	0.512	3.520	2.119	1.772
5.72 (5000)	This Study	FTW	1.208	1.296	1.592	2.455	3.882	5.758
	Experimental		1.317 (1152)	1.173 (1026)	1.581 (1383)	2.385 (2086)	3.824 (3344)	5.694 (4980)
	Error %		8.267	10.481	0.666	2.924	1.537	1.119
	This Study	BTW	1.208	1.106	1.211	1.883	3.120	4.805
	Experimental		1.317 (1152)	0.988 (864)	1.243 (1087)	1.817 (1589)	3.070 (2685)	4.748 (4152)
	Error %		8.267	11.906	2.588	3.649	1.628	1.214
8.58 (7500)	This Study	FTW	1.215	1.351	1.697	2.607	4.081	6.004
	Experimental		1.325 (1159)	1.229 (1075)	1.669 (1460)	2.534 (2216)	4.026 (3521)	5.934 (5190)
	Error %		8.328	9.950	1.638	2.894	1.374	1.170
	This Study	BTW	1.215	1.066	1.125	1.750	2.938	4.575
	Experimental		1.325 (1159)	0.949 (830)	1.131 (989)	1.688 (1476)	2.896 (2533)	4.526 (3958)
	Error %		8.328	12.284	0.515	3.667	1.436	1.079

The minimum error is 0.512% in the mode (0,2) for the dimensionless rotational speed of 2.86 which corresponds to 2500 rpm and the maximum error is 11.906% in the

mode (0,1) for the dimensionless rotational speed of 5.72 which corresponds to 5000 rpm. Overall, the results show significant consistency.

5. CONCLUSION

The principal goal of this study is to investigate the transverse vibrations of a spinning disk under various boundary conditions and the effects of the rotational speed and the radius ratio on the frequency. To determine the free vibration behaviour of spinning disks, a five-term polynomial function is chosen as the approximate solution and the Galerkin method is applied. The unknown parameters are procured from the boundary and normalization circumstances then the natural frequencies are calculated. For the comparison purpose, the results of the FE analysis is presented. Furthermore, the effects of different rotational speeds and radius ratios on dimensionless frequency is studied. Obtained results are visualised with 3D surfaces.

The variation of the natural frequencies of a spinning disk strongly depends on the boundary conditions. Another important parameter is the radius ratio of the inner and outer circumferences. In most of the modes where tension is dominant throughout the disk, the increasing radius ratio stiffens the structure and leads to a consistent increase in the natural frequencies of the disk. The only exception to this is the free disk. Most of the modes of the free disk are insensitive to the change of radius ratio and some of the modes slightly shift upward with decreasing radius ratio. In the compression dominant disks, this softening is visible as well. However, this softening can stop and the disk can start to behave stiffer due to changes in stresses in the disk after some radius ratios, in other words, an extremum is observed for a specific radius ratio value.

The results show that both the Galerkin, the FEM and the experimental methods produce consistent results. The maximum error between the FEM and the analytical

method is around 10% and the majority of the results fall within a margin of 2%. More important than the errors, the trends of the results match very well in both methods.

REFERENCES

Amabili, M., Pierandrei, R., and Frosali, G., 1997. Analysis of vibrating circular plates having non-uniform constraints using the modal properties of free-edge plates: Application to bolted plates. *Journal of Sound and Vibration*, 206 (1), 23–38.

Barasch, S. and Chen, Y., 1972. On the vibration of a rotating disk. *Journal of Applied Mechanics, Transactions ASME*, 39 (4), 1143–1144.

Bashmal, S., Bhat, R., and Rakheja, S., 2016. Experimental and numerical study of the vibration of stationary and rotating annular disks. *Journal of Vibration and Acoustics, Transactions of the ASME*, 138 (5), 1–11.

Cicirello, A. and Langley, R.S., 2013. The vibro-acoustic analysis of built-up systems using a hybrid method with parametric and non-parametric uncertainties. *Journal of Sound and Vibration*, 332 (9), 2165–2178.

Cicirello, A. and Langley, R.S., 2014. Efficient parametric uncertainty analysis within the hybrid Finite Element/Statistical Energy Analysis method. *Journal of Sound and Vibration*, 333 (6), 1698–1717.

Guo, H., Zhuang, X., and Rabczuk, T., 2019. A deep collocation method for the bending analysis of Kirchhoff plate. *Computers, Materials and Continua*, 59 (2), 433–456.

Güven, U. and Çelik, A., 2001. On transverse vibrations of functionally graded isotropic linearly elastic rotating solid disks. *Mechanics Research Commumcations*, 28 (3), 271–276.

Huang, S.C. and Hsu, B.S., 1992. Theory of receptance applied to modal analysis of a spinning disk with interior multi-point supports. *Journal of Vibration and*

Acoustics, Transactions of the ASME, 114 (4), 468–476.

Huang, S.C. and Lin, K.A., 2008. Vibration characteristics of computer stacked disks and head assembly. *Journal of Mechanical Science and Technology*, 22 (3), 460–468.

Jaiman, Y. and Singh, B., 2019. Free vibration of circular annular plate with different boundary conditions. *Vibroengineering Procedia*, 29 (1), 82–86.

Kajiwara, I. and Hosoya, N., 2013. Vibration measurement and monitoring of a rotating disk using contactless laser excitation. *In*: *ASME 2013 Dynamic Systems and Control Conference, DSCC 2013*. 1–5.

Kang, J.H., 2017. Axisymmetric Vibration of Rotating Annular Plate with Variable Thickness Subjected to Tensile Centrifugal Body Force. *International Journal of Structural Stability and Dynamics*, 17 (9), 1–18.

Kim, C.S. and Lee, C.W., 1988. Travelling wave control of rotating discs and analysis of its spillover effect. *Proceedings of the Institution of Mechanical Engineers, Part C: Journal of Mechanical Engineering Science*, 202 (2), 119–127.

Kirkhope, J. and Wilson, G.J., 1976. A finite element analysis for the vibration modes of a bladed disc. *Journal of Sound and Vibration*, 49 (4), 469–482.

Koo, K.N., 2006. Vibration analysis and critical speeds of polar orthotropic annular disks in rotation. *Composite Structures*, 76 (1–2), 67–72.

Kutug, Z., Yahnioglu, N., and Akbarov, S.D., 2003. The loss of stability analyses of an elastic and viscoelastic composite circular plate in the framework of three-dimensional linearized theory. *European Journal of Mechanics, A/Solids*, 22 (3), 475–488.

Lamb, H. and Southwell, R. V., 1921. Transverse Vibrations of a Uniform Circular Disc. *Proceeding of the Royal Society, Series A Mathematical, Physical and*

Engineering Sciences, 59, 133–153.

Luo, A.C.J. and Mote, C.D., 2000. Nonlinear vibration of rotating thin disks. *Journal of Vibration and Acoustics, Transactions of the ASME*, 122 (4), 376–383.

Lyu, P., Du, J., Wang, Y., and Liu, Z., 2019. Free in-plane vibration analysis of rotating annular panels with elastic boundary restraints. *Journal of Sound and Vibration*, 439, 434–456.

Maretic, R., Glavardanov, V., and Milosevic-Mitic, V., 2015. Vibration and stability of rotating annular disks composed of different materials. *Archive of Applied Mechanics*, 85 (1), 117–131.

Mattikalli, A.C. and Kurahatti, R. V., 2018. Finite element analysis of free vibration of an annular plate. *In*: *AIP Conference Proceedings*.

Mignolet, M.P., Eick, C.D., and Harish, M. V., 1996. Free vibration of flexible rotating disks. *Journal of Sound and Vibration*, 196 (5), 537–577.

Mote, C.D., 1965. Free vibration of initially stressed circular disks. *Journal of Manufacturing Science and Engineering, Transactions of the ASME*, 87 (2), 258–264.

Nayfeh, A.H., Jilani, A., and Manzione, P., 2001. Transverse vibrations of a centrally clamped rotating circular disk. *Nonlinear Dynamics*, 26 (2), 163–178.

Nguyen-Thanh, N., Thai-Hoang, C., Nguyen-Xuan, H., and Rabzcuk, T., 2009. A smoothed finite element method for the static and free vibration analysis of shells. *Journal of Civil Engineering and Architecture*, (February 2016), 1–24.

Oldac, O., Tufekci, M., Genel, O.E., and Tufekci, E., 2017. Free Bending Vibrations of Rotating Disks With A Concentric Hole. *International Journal of Technology and Engineering Studies*, 3 (6), 253–263.

Panunzio, A.M., Salles, L., and Schwingshackl, C.W., 2017. Uncertainty propagation

for nonlinear vibrations: A non-intrusive approach. *Journal of Sound and Vibration*, 389, 309–325.

Parker, R.G. and Sathe, P.J., 1999a. Free vibration and stability of a spinning disk–spindle system. *Journal of Vibration and Acoustics, Transactions of the ASME*, 121 (3), 391–396.

Parker, R.G. and Sathe, P.J., 1999b. Exact solutions for the free and forced vibration of a rotating disk-spindle system. *Journal of Sound and Vibration*, 223 (3), 445–465.

Pei, Y.C. and Tan, Q.C., 2009. Modal interactions in a rotating flexible disc. *Proceedings of the Institution of Mechanical Engineers, Part C: Journal of Mechanical Engineering Science*, 223 (4), 851–857.

Qin, X., Jin, G., Chen, M., and Yin, S., 2018. Free In-Plane Vibration Analysis of Circular, Annular, and Sector Plates Using Isogeometric Approach. *Shock and Vibration*, 2018.

Ramaiah, G.K., 1981. Natural frequencies of spinning annular plates. *Journal of Sound and Vibration*, 74 (2), 303–310.

Samaniego, E., Anitescu, C., Goswami, S., Nguyen-Thanh, V.M., Guo, H., Hamdia, K., Zhuang, X., and Rabczuk, T., 2020. An energy approach to the solution of partial differential equations in computational mechanics via machine learning: Concepts, implementation and applications. *Computer Methods in Applied Mechanics and Engineering*, 362, 112790.

Shafei, E., Faroughi, S., and Rabczuk, T., 2021. Nonlinear transient vibration of viscoelastic plates: A NURBS-based isogeometric HSDT approach. *Computers and Mathematics with Applications*, 84, 1–15.

Southwell, R. V., 1922. On the free transverse vibrations of a uniform circular disc clamped at its centre; and on the effects of rotation. *Proceedings of the Royal*

Society of London. Series A, Containing Papers of a Mathematical and Physical Character, 101 (709), 133–153.

Sun, Y., Yuan, J., Pesaresi, L., Denimal, E., and Salles, L., 2020. Parametric study and uncertainty quantification of the nonlinear modal properties of frictional dampers. *Journal of Vibration and Acoustics, Transactions of the ASME*, 142 (5).

Tufekci, M., Genel, O.E., Koc, H., Oldac, O., and Tufekci, E., 2019. Vibrations of a rotating disk under perpendicular spacefixed forces. *Gazi University Journal of Science*, 32 (1), 273–284.

Tufekci, M., Genel, O.E., and Oldac, O., 2017. Experimental and finite element analysis of vibrations of a rotating annular plates. *Journal of Advances in Technology and Engineering Research*, 3 (6), 224–234.

Tufekci, M., Koc, H., Genel, O.E., and Oldac, O., 2018. Free transverse vibrations of rotating annular disks under various boundary conditions. *Sigma Journal of Engineering and Natural Sciences*, 9 (2), 243–255.

Tufekci, M., Rendu, Q., Yuan, J., Dear, J.P., Salles, L., and Cherednichenko, A. V., 2020. Stress and modal analysis of a rotating blade and the effects of nonlocality. *In*: *Proceedings of the ASME Turbo Expo*. American Society of Mechanical Engineers, 1–12.

Tuzzi, G., Schwingshackl, C.W., and Green, J.S., 2020. Study of coupling between shaft bending and disc zero nodal diameter modes in a flexible shaft-disc assembly. *Journal of Sound and Vibration*, 479, 115362.

Vu-Bac, N., Lahmer, T., Zhuang, X., Nguyen-Thoi, T., and Rabczuk, T., 2016. A software framework for probabilistic sensitivity analysis for computationally expensive models. *Advances in Engineering Software*, 100, 19–31.

Xu, L.M. and Guo, N., 2003. Modal testing and finite element modelling of subsystem

in hard disk drive. *Mechanical Systems and Signal Processing*, 17 (4), 747–764.

Yano, S. and Kotera, T., 1991. Instability of the vibrations of a rotating thin disk due to an additional support. *Archive of Applied Mechanics*, 61 (2), 110–118.

Yıldırım, V., 2018. Numerical/analytical solutions to the elastic response of arbitrarily functionally graded polar orthotropic rotating discs. *Journal of the Brazilian Society of Mechanical Sciences and Engineering*, 40 (6).

Yıldırım, V., 2020. The best grading pattern selection for the axisymmetric elastic response of pressurized inhomogeneous annular structures (sphere/cylinder/annulus) including rotation. *Journal of the Brazilian Society of Mechanical Sciences and Engineering*, 42 (2), 1–19.

DISCLOSURE STATEMENT

No potential competing interest was reported by the authors.